AIAA JOURNAL
Vol. 30, No. 6, June 1992

# High-Resolution, Nonoscillatory Schemes for Unsteady Compressible Flows

J. Y. Yang* and C. A. Hsu†
*National Taiwan University, Taipei, Taiwan 10764, Republic of China*

**High-resolution explicit finite difference nonoscillatory shock-capturing schemes based on Harten's essentially nonoscillatory interpolation using reconstruction via primitive function approach with $N = 3$ are described for simulating unsteady compressible flows. The extension to nonlinear system is done by using Roe's method, which permits the use of different scalar schemes for different characteristic fields. For multidimensional problems, Strang-type dimensional splitting is adopted. Numerical simulations of unsteady shock diffraction by an elliptic cylinder and shock wave propagating through a convergent-divergent nozzle are included to illustrate the performance of the schemes.**

## I. Introduction

YEE[1] gives a very extensive survey of the state-of-the-art of second-order high-resolution schemes for the Euler/Navier-Stokes equations of gas dynamics in general coordinates for both ideal and equilibrium real gases. Also, excellent reviews on modern upwind conservative shock-capturing schemes and upwind shock-fitting schemes based on wave propagation property have been given by Roe[2] and Moretti[3], respectively.

Recently, a new class of uniformly high-order-accurate, essentially nonoscillatory (ENO) schemes have been developed by Harten and Osher,[4] Harten et al.[5-7]. They presented a hierarchy of uniformly high-order-accurate schemes that generalize Godunov's scheme,[8] and its second-order-accurate extension of monotonic upstream schemes for conservation laws (MUSCL)[9,10] and total variation diminishing (TVD) schemes[11-13] to arbitrary order of accuracy.

In contrast to the earlier second-order TVD schemes, which drop to first-order accuracy at local extrema and maintain second-order accuracy in smooth regions, the new ENO schemes are uniformly high-order accurate throughout even at critical points. Theoretical results for the scalar coefficient case and numerical results for the scalar conservation law and for the Euler equations of gas dynamics have been reported with highly accurate results. Preliminary results for two-dimensional problems were reported in.[5] Second and third-order nonoscillatory schemes for the Euler equations in general curvilinear coordinates using the modified flux approach[11] have been given in Refs. 14 and 15.

In this paper, following Harten and Osher,[4-7] we describe a class of third-order (at least one-dimensional scalar case) shock capturing ENO schemes for the Euler equations of gas dynamics. Third-order schemes are constructed using ENO interpolation. The development is identical to those given in Ref. 15 except that the Roe's approximate Riemann solver[16] is employed here instead of the characteristic flux difference splitting method. The main difference between the approach used in Ref 15 and the present work lies in that the former one operates on the difference of flux vector, whereas the present one operates on the difference of conservative state vector. It is known that the conservative vector is not continuous across the shock whereas the flux is continuous; that is the flux vector function is one order smoother than the conservative state vector function. The Roe's averages[14] enable the Rankine-Hugoniot relations to be satisfied across the shock. Also, the Roe's linearization technique for nonlinear system permits the use of completely different scalar schemes for different characteristic fields and is one of the most popular approximate Riemann solvers currently in use.

We apply the resulting schemes to simulate one- and two-dimensional unsteady gasdynamic flows involving strong shock interactions to illustrate the performance of the schemes.

In Sec. II, characteristic properties of the Euler equations related to the numerical advections are briefly summarized.

In Sec. III, the essentially nonoscillatory interpolation of Harten, Osher, Engquist and Chakravarthy[4-7] using reconstruction via primitive function approach for $N = 3$ is employed to yield a third order nonoscillatory scheme.

In Sec. IV, explicit nonoscillatory schemes for the two-dimensional Euler equations in general coordinates are outlined.

Numerical experiments with the proposed third-order schemes for solving shock diffraction by an elliptic cylinder and shock wave propagating through a convergent-divergent nozzle are presented in Sec. V.

Conclusions are given in Sec. VI.

## II. Euler Equations and Roe Scheme

Consider the one-dimensional Euler equations of inviscid gas dynamics in conservation law form:

$$\partial_t Q + \partial_x F(Q) = 0 \tag{1}$$

where $Q = (\rho, \rho u, e)^T$ is the conservative state vector and $F = (\rho u, \rho u^2 + p, u(e + p))^T$ the flux vector. Here $\rho$ is the fluid density, $u$ the fluid velocity, $p$ the fluid pressure, and $e$ the total internal energy. For a perfect gas, the pressure is related to other fluid properties by the equation of state $p = (\gamma - 1)(e - \rho u^2/2)$, where $\gamma$ is the ratio of the specific heats.

Eq. (1) can be expressed in quasilinear form as:

$$\partial_t Q + A(Q)\, \partial_x Q = 0 \tag{2}$$

where $A$ is the Jacobian matrix $\partial F/\partial Q$ and has real eigenvalues:

$$(a_1, a_2, a_3) = (u - c, u, u + c) \tag{3}$$

where $c = \sqrt{\gamma p/\rho}$ is the sound speed.

Received Oct. 16, 1990; revision received Aug. 8, 1991; accepted for publication Aug. 19, 1991. 

*Associate Professor, Institute of Applied Mechanics. Member AIAA.
†Graduate Student, Institute of Applied Mechanics.

Define a uniform mesh $\{x_j, t^n\}$, with mesh size $\Delta x$ and $\Delta t$ and $\lambda = \Delta t/\Delta x$ is the mesh ratio. Define the Courant number:

$$\sigma_l = a_l \Delta t/\Delta x = a_l \lambda \tag{4}$$

A conservative scheme for Eq. (1) based on Roe's method[16] with some entropy fix due to Harten can be written as:

$$Q_j^{n+1} = Q_j^n - \lambda[F_{j+1/2}^N - F_{j-1/2}^N] \tag{5}$$

where $F_{j+1/2}^N$ is the numerical flux and defined by:

$$F_{j+1/2}^N = \tfrac{1}{2}[F_j^n + F_{j+1}^n + R_{j+1/2}\Phi_{j+1/2}] \tag{6}$$

Here for the first order upwind scheme, the components of the column vector $\mathbf{\Phi}_{j+1/2}$ are given by:

$$\phi_{j+1/2}^l = -\psi(a_{j+1/2}^l)\alpha_{j+1/2}^l \tag{7}$$

where

$$\alpha_{j+1/2} = L_{j+1/2}(Q_{j+1} - Q_j) \tag{8}$$

and

$$\psi(z) = \begin{cases} |z|, & \text{if } |z| \geq \varepsilon \\ (z^2 + \varepsilon^2)/2\varepsilon & \text{if } |z| < \varepsilon \end{cases} \tag{9}$$

where $\varepsilon$ is some small number. Eq. (9) is the so-called entropy fix and is applied only to the genuinely nonlinear eigenvalues $a_1$ and $a_3$. The right and left eigenvector matrices $R$ and $L$ in Eq. (6) and Eq. (8) are given by

$$R = \begin{bmatrix} 1 & 1 & 1 \\ u - c & u & u + c \\ H - uc & \tfrac{1}{2}u^2 & H + uc \end{bmatrix} \tag{10}$$

$$L = \begin{bmatrix} \tfrac{1}{2}(b_2 + u/c) & -\tfrac{1}{2}(ub_1 + 1/c) & \tfrac{1}{2}b_1 \\ 1 - b_2 & b_1 u & -b_1 \\ \tfrac{1}{2}(b_2 - u/c) & -\tfrac{1}{2}(ub_1 - 1/c) & \tfrac{1}{2}b_1 \end{bmatrix} \tag{11}$$

where $b_1 = (\gamma - 1)c^2$ and $b_2 = \tfrac{1}{2}u^2 b_1$ and $H = (e + p)/\rho = c^2/(\gamma - 1) + \tfrac{1}{2}u^2$ is the total enthalpy.

The Roe's averages are defined as

$$\bar{\rho} = D\rho_j \tag{12a}$$

$$\bar{u} = \frac{u_j + Du_{j+1}}{1 + D} \tag{12b}$$

$$\bar{H} = \frac{H_j + DH_{j+1}}{1 + D} \tag{12c}$$

$$\bar{c}^2 = (\gamma - 1)[\bar{H} - \tfrac{1}{2}\bar{u}^2] \tag{12d}$$

$$D = \sqrt{\rho_{j+1}/\rho_j} \tag{12e}$$

In the following, we shall give third-order nonoscillatory schemes for Eq. (1) in the form of Eq. (5) and Eq. (6) with a new expression $\Phi_{j+1/2}^{UNO3}$. That is to give expressions of $\Phi$ that achieve high-order accuracy and yield nonoscillatory solutions.

## III. Third-Order Nonoscillatory Schemes

In this section, we briefly describe the basic element of the essentially nonoscillatory schemes due to Harten et al.

Harten and Osher[4] introduced a new class of nonoscillatory schemes that are of uniformly high-order accuracy. Unlike TVD schemes, nonoscillatory schemes are not required to damp the values of each local extremum at every single time-step, but are allowed to occasionally accentuate a local extremum. The design involves an essentially nonoscillatory piecewise polynomial reconstruction of the solution from its cell averages, time evolution through an approximate solution of the resulting initial value problem, and averaging of this approximate solution over each cell. For further details, the reader is encouraged to read their original papers.[4-7]

### Essentially Nonoscillatory Interpolation

For illustration purposes, we first consider the following scalar wave equation as the model equation for Eq. (2):

$$\partial_t u + a\partial_x u = 0, \quad a > 0 \tag{13}$$

Using reconstruction via the primitive function (RP) approach and for $N = 3$, one has a numerical scheme for Eq. (13):

$$v_j^{n+1} = v_j^n - \sigma\Delta_- v_j^n - \sigma\Delta_-\left[\left(\frac{1 - \sigma}{2}\right)m(\Delta_- v_j^n, \Delta_+ v_j^n)\right] - \begin{cases} \sigma\Delta_-\left[\dfrac{(2 - 3\sigma + \sigma^2)}{6}\,\overline{m}(\Delta_-\Delta_- v_j^n, \Delta_-\Delta_+ v_j^n)\right] \\ \qquad \text{if } |\Delta_- v_j^n| \leq |\Delta_+ v_j^n| \\ \sigma\Delta_-\left[\dfrac{(\sigma^2 - 1)}{6}\,\overline{m}(\Delta_-\Delta_+ v_j^n, \Delta_+\Delta_+ v_j^n)\right] \\ \qquad \text{if } |\Delta_- v_j^n| > |\Delta_+ v_j^n| \end{cases} \tag{14}$$

In Eq. (14), $\sigma = a\lambda$ and $m$ and $\overline{m}$ functions are defined, for any two real numbers $y$ and $z$, by:

$$m(y, z) = \begin{cases} s\min(|y|, |z|), & \text{if } \operatorname{sgn} y = \operatorname{sgn} z = s \\ 0, & \text{otherwise} \end{cases} \tag{15}$$

$$\overline{m}(y, z) = \begin{cases} y, & \text{if } |y| \leq |z| \\ z, & \text{if } |y| > |z| \end{cases} \tag{16}$$

A third-order ENO scheme for Eq. (1) based on Eq. (14) can be expressed in the form of Eq. (6) in terms of the numerical flux:

$$F_{j+1/2}^{UNO3} = \tfrac{1}{2}[F_j + F_{j+1} + R_{j+1/2}\Phi_{j+1/2}^{UNO3}] \tag{17}$$

The components of $\Phi_{j+1/2}^{UNO3}$ are defined as:

$$\phi_{j+1/2}^{l\ UNO3} = \sigma(a_{j+1/2}^l)(\beta_j^l + \beta_{j+1}^l) + \begin{cases} \tilde{\sigma}(a_{j+1/2}^l)(\tilde{\beta}_j^l + \tilde{\beta}_{j+1}^l) - \psi(a_{j+1/2}^l + \gamma_{j+1/2}^l + \tilde{\gamma}_{j+1/2}^l)\alpha_{j+1/2}^l \\ \qquad \text{if } |\alpha_{j-1/2}^l| \leq |\alpha_{j+1/2}^l| \\ \hat{\sigma}(a_{j+1/2}^l)(\hat{\beta}_j^l + \hat{\beta}_{j+1}^l) - \psi(a_{j+1/2}^l + \gamma_{j+1/2}^l + \hat{\gamma}_{j+1/2}^l)\alpha_{j+1/2}^l \\ \qquad \text{otherwise} \end{cases} \tag{18}$$

where the $\sigma$, $\tilde{\sigma}$, and $\hat{\sigma}$ functions are given by:

$$\sigma(z) = \tfrac{1}{2}[\psi(z) - \lambda z^2] \tag{19}$$

$$\tilde{\sigma}(z) = \tfrac{1}{6}[2|z| - 3\lambda|z|^2 + \lambda^2|z|^3] \tag{20}$$

$$\hat{\sigma}(z) = \tfrac{1}{6}[\lambda^2|z|^3 - |z|] \tag{21}$$

and

$$\beta_j^l = m[\alpha_{j+1/2}^l, \alpha_{j-1/2}^l] \tag{22}$$

$$\tilde{\beta}_j^l = \overline{m}[\Delta_-\alpha_{j-1/2}^l, \Delta_+\alpha_{j-1/2}^l] \quad \text{if } |\alpha_{j-1/2}^l| \leq |\alpha_{j+1/2}^l| \tag{23}$$

$$\hat{\beta}_j^l = \overline{m}[\Delta_-\alpha_{j+1/2}^l, \Delta_+\alpha_{j+1/2}^l] \quad \text{if } |\alpha_{j-1/2}^l| > |\alpha_{j+1/2}^l| \tag{24}$$

$$\gamma^l_{j+1/2} = \sigma(a^l_{j+1/2}) \begin{cases} (\beta^l_{j+1} - \beta^l_j)/\alpha^l_{j+1/2}, & \text{if } \alpha^l_{j+1/2} \neq 0 \\ 0, & \text{otherwise} \end{cases} \quad (25)$$

$$\tilde{\gamma}^l_{j+1/2} = \tilde{\sigma}(a^l_{j+1/2}) \begin{cases} (\tilde{\beta}^l_{j+1} - \tilde{\beta}^l_j)/\alpha^l_{j+1/2}, & \text{if } \alpha^l_{j+1/2} \neq 0 \\ 0, & \text{otherwise} \end{cases} \quad (26)$$

$$\hat{\gamma}^l_{j+1/2} = \hat{\sigma}(a^l_{j+1/2}) \begin{cases} (\hat{\beta}^l_{j+1} - \hat{\beta}^l_j)/\alpha^l_{j+1/2}, & \text{if } \alpha^l_{j+1/2} \neq 0 \\ 0, & \text{otherwise} \end{cases} \quad (27)$$

For comparison purposes, we also list the second-order TVD and ENO schemes as follows:

$$\phi^l_{j+1/2}{}^{ENO2} = \sigma(a^l_{j+1/2})(\bar{\beta}^l_j + \bar{\beta}^l_{j+1}) - \psi(a^l_{j+1/2} + \bar{\gamma}^l_{j+1/2})\alpha^l_{j+1/2} \quad (28)$$

where

$$\bar{\beta}^l_j = m[\alpha^l_{j+1/2} - \zeta\, \overline{m}(\Delta_+\alpha^l_{j+1/2}, \Delta_-\alpha^l_{j+1/2}), \alpha^l_{j-1/2} + \zeta\, \overline{m}(\Delta_+\alpha^l_{j-1/2}, \Delta_-\alpha^l_{j-1/2})] \quad (29)$$

and

$$\bar{\gamma}^l_{j+1/2} = \sigma(a^l_{j+1/2}) \begin{cases} \bar{\beta}^l_{j+1} - \bar{\beta}^l_j)/\alpha^l_{j+1/2}, & \text{if } \alpha^l_{j+1/2} \neq 0 \\ 0, & \text{otherwise} \end{cases} \quad (30)$$

For $\zeta = 0$, one has a second-order TVD scheme[11] and for $\zeta = \frac{1}{2}$, one has a uniformly second-order essentially nonoscillatory scheme.[4] We denote them as TVD2 and ENO2 schemes.

## IV. Euler Equations in General Coordinates

We consider the conservation equations of the two-dimensional unsteady gas dynamics in general coordinates $\xi$, $\eta$:

$$\partial_t Q + \partial_\xi F + \partial_\eta G = 0 \quad (31)$$

where

$$Q = J^{-1}\begin{pmatrix} \rho \\ \rho u \\ \rho v \\ e \end{pmatrix}, \qquad F = J^{-1}\begin{pmatrix} \rho U \\ \rho u U + \xi_x p \\ \rho v U + \xi_y p \\ U(e + p) \end{pmatrix}$$

$$G = J^{-1}\begin{pmatrix} \rho V \\ \rho u V + \eta_x p \\ \rho v V + \eta_y p \\ V(e + p) \end{pmatrix} \quad (32)$$

and

$$U = \xi_x u + \xi_y v, \qquad V = \eta_x u + \eta_y v \quad (33)$$

Here, $\rho$ is the fluid density, $u$ and $v$ are velocity components in $x$ and $y$ direction, and $e$ is the total internal energy, and $p$ is the pressure and is related to other variables by $p = (\gamma - 1)[e - \rho(u^2 + v^2)/2]$ where $\gamma$ is the ratio of specific heats. The metric Jacobian and the metric terms are given by:

$$J = \xi_x\eta_y - \xi_y\eta_x \quad (34)$$

$$\xi_x = Jy_\eta, \qquad \xi_y = -Jx_\eta \quad (35a)$$

$$\eta_x = -J_{y\xi}, \qquad \eta_y = Jx_\xi \quad (35b)$$

The Jacobian coefficient matrices $A_\xi = \partial F/\partial Q$ and $B_\eta$ and $\partial G/\partial Q$ of the transformed equations have real eigenvalues:

$$(a_1, a_2, a_3, a_4) = (U - c_\xi, U, U + c_\xi, U) \quad (36a)$$

and

$$(b_1, b_2, b_3, b_4) = (V - c_\eta, V, V + c_\eta, V) \quad (36b)$$

with $c_\xi = c\sqrt{\xi_x^2 + \xi_y^2}$ and $c_\eta = c\sqrt{\eta_x^2 + \eta_y^2}$, where $c\sqrt{\gamma p/\rho}$ is the speed of sound.

One can also find similarity transformation matrices, $R^\xi$, and $R^\eta$ and their inverses $L^\xi$ and $L^\eta$ that diagonalize $A_\xi$ and $B_\eta$:

$$L^\xi A_\xi R^\xi = \Lambda_\xi = \text{diag}\{a_l\}, \quad L^\eta B_\eta R^\eta = \Lambda_\eta = \text{diag}\{b_l\} \quad (37)$$

Define a uniform computational mesh system $(\xi_j, \eta_k)$ with mesh sizes $\Delta\xi = \Delta\eta = 1$ and let $Q^n_{j,k}$ denote the value of $Q$ at time level $n\Delta t$ and at position $(j\Delta\xi, k\Delta\eta)$. Define the difference of the characteristic variables in the local $\xi$ direction and $\eta$ direction respectively as:

$$\alpha^\xi_{j+1/2,k} = L^\xi_{j+1/2,k}(\hat{Q}_{j+1,k} - \hat{Q}_{j,k})$$

$$\alpha^\eta_{j,k+1/2} = L^\eta_{j,k+1/2}(\hat{Q}_{j,k+1} - \hat{Q}_{j,k}) \quad (38)$$

where $\hat{Q} = JQ = (\rho, \rho u, \rho v, e)^T$. Similar to the one-dimensional case given before, we have a conservative scheme for Eq. (31) as:

$$Q^{n+1}_{j,k} = Q^n_{j,k} - \Delta t[F^N_{j+1/2,k} - F^N_{j-1/2,k}] - \Delta t[G^N_{j,k+1/2} - G^N_{j,k-1/2}] \quad (39)$$

To construct a properly multidimensional upwind scheme for solving Eq. (39) is highly desirable and is currently under extensive study. It is customary to adopt Strang-type dimensional splitting technique[17], where the individual operators act along rows and columns of the mesh. An investigation on splitting error of dimensional splitting and the proper multidimensional wave recognition techniques was given by Roe.[18]

In this work, for explicit upwind methods in two space dimensions, the Strang-type dimensional splitting was employed.

$$Q^{n+2}_{j,k} = \mathcal{L}_\xi(\Delta t)\mathcal{L}_\eta(\Delta t)\mathcal{L}_\eta(\Delta t)\mathcal{L}_\xi(\Delta t)Q^n_{j,k} \quad (40)$$

The one-dimensional $\mathcal{L}_\xi$ operator is defined by:

$$\mathcal{L}_\xi Q^n_{j,k} = Q^n_{j,k} - \Delta t(F^{UNO3}_{j+1/2,k} - F^{UNO3}_{j-1/2,k}) \quad (41)$$

with

$$F^{UNO3}_{j+1/2,k} = \tfrac{1}{2}[F^n_{j,k} + F^n_{j+1,k} + R^\xi_{j+1/2,k}\Phi^{UNO3}_{j+1/2,k}/J_{j+1/2,}] \quad (42)$$

where all the metric terms $(\xi_x)_{j+1/2,k}$ and $(\xi_y)_{j+1/2,k}$ used in $R^\xi_{j+1/2,k}$ and $J_{j+1/2,k}$ are evaluated using simple averages

$$(\xi_x)_{j+1/2,k} = \tfrac{1}{2}[(\xi_x)_{j,k} + (\xi_x)_{j+1,k}]$$

$$J_{j+1/2,k} = \tfrac{1}{2}(J_{j,k} + J_{j+1,k}) \quad (43)$$

The components of $\Phi^{UNO3}_{j+1/2,k}$ can be expressed in the same way as Eq. (18). The $\sigma$, $\tilde{\sigma}$, and $\hat{\sigma}$ functions corresponding to those defined in Eqs. (19–21) can be obtained by replacing $\lambda$ by $\Delta t$. The expressions for $\gamma^l$'s and $\beta^l$'s functions are similarly defined.

Similarly, one can define the $\mathcal{L}_\eta$ operator and the numerical flux $G^{UNO3}_{j,k+1/2}$ in the $\eta$ direction.

The boundary conditions at the walls used are exactly the same as those given in Ref. 19, which employ the Riemann invariants and permit integration of the equations from boundary to boundary and produce very clean profile at the boundaries.

For the explicit third-order scheme in two dimensions, we still employ the dimensional splitting. Although some splitting errors may be introduced and the scheme can no longer claim

to be of third-order accuracy, however, the numerical simulations given in next section indicate that such a procedure works well, particularly for unsteady flows.[18]

## V. Numerical Results and Discussions

Results of several numerical experiments are given in this section to illustrate some characteristics of the present third order nonoscillatory schemes as applied to one-dimensional and two-dimensional unsteady gasdynamic problems with strong shocks.

### Interaction of Blast Waves

We first present numerical experiments with the third-order nonoscillatory scheme for the problem of two interacting blast waves suggested by Woodward and Colella as a test problem; we refer the reader to Ref. 20 where a comprehensive comparison of the performance of various schemes for this problem is presented. The initial states are given by

$$Q(x, 0) = \begin{cases} Q_L, & \text{if } 0.0 \le x < 0.1 \\ Q_M, & \text{if } 0.1 \le x < 0.9 \\ Q_R, & \text{if } 0.9 \le x < 1.0 \end{cases}$$

where

$$\rho_L = \rho_M = \rho_R = 1, \qquad u_L = u_M = u_R = 0$$

$$p_L = 10^3, \qquad p_M = 10^{-2}, \qquad p_R = 10^2$$

For comparison purposes, we also include the results obtained using the second-order schemes TVD2 and ENO2 defined by Eq. (28). The entropy parameter $\varepsilon$ was taken to be zero in this one-dimensional problem. Figures 1–3 indicate the computed solutions (circles) of density obtained using TVD2, ENO2, and UNO3 schemes. The solid line is the "exact" solution taken from Ref. 20. Using a uniform grid system of 400 points and CFL = 0.99, the CPU time required to reach time $t = 0.038$ is 21.55 s for TVD2 scheme; 22.62 s for ENO2 scheme; and 29.56 s for UNO3 scheme on a Convex C-1 computer.

Here we have used Eqs. (23) and (24) with the $\overline{m}$ function replaced by the minmod function $m$. Comparing these solutions to the "exact" solution of Woodward and Colella[20], we find that all the important features of the various interactions were captured. The UNO3 and ENO2 results represent the three contact discontinuities better than the TVD2 results do.

### Shock Wave Reflection by an Elliptic Cylinder

In this problem we consider a plane shock wave, located initially at a certain distance ahead of the elliptic cylinder, propagates with shock Mach number $M_s$ toward the elliptic cylinder and experiences truly nonstationary shock reflection. All the calculations are done using UNO3 scheme. We first validate the code by comparing the computed results with available experimental photographs. Shown in Fig. 4 is a comparison of computed density contours and a holographic interferogram. The shock Mach number is $M_s = 1.7$ and the semi-axes of the ellipse are 1.0 and 0.5 respectively. A grid system of 721 × 201 was used. The entropy parameter $\varepsilon = 0.125$ was used on $U \pm c_\xi$ and $V \pm c_\eta$. Very good agreement can be observed. Second, a grid convergence check with two grid systems of size 361 × 101 and 721 × 201 is also shown in Fig. 5 for a shock Mach number $M_s = 2.81$ and semi-axes of the ellipse are 0.75 and 0.5. It is noted that the roll-up of the slipline and vortex are much clearly captured by using the finer mesh. Due to the lack of length scales for the inviscid compressible Euler equations, one has to decide and choose a suitable mesh system to present a physical problem. In this

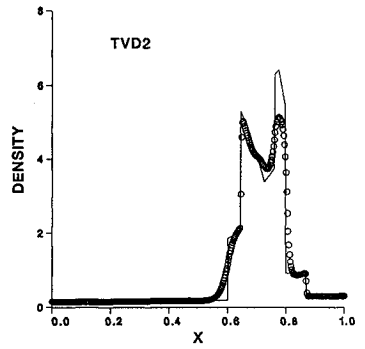


Fig. 1 Solution of one-dimensional interacting blast waves, TVD2 scheme.

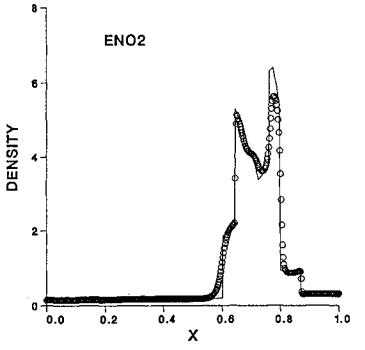


Fig. 2 Solution of one-dimensional interacting blast waves, ENO2 scheme.

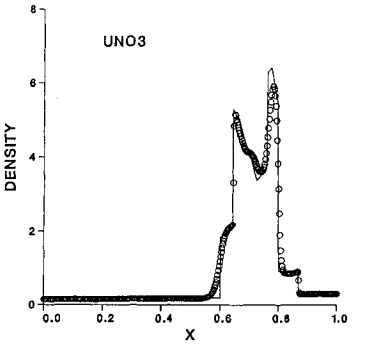


Fig. 3 Solution of one-dimensional interacting blast waves, UNO3 scheme.

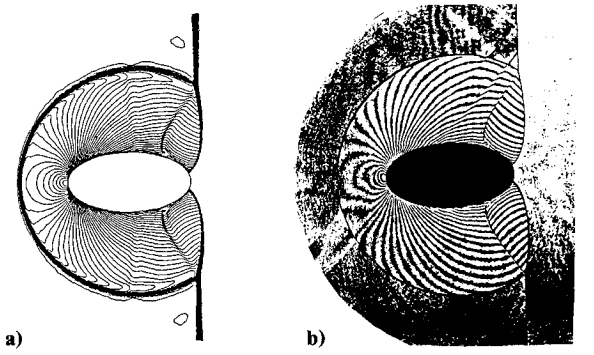


Fig. 4 Comparison of computed solution and experimental result $M_s = 1.7$ a) computed density contours, b) holographic interferogram (courtesy of K. Takayama, Tohoku University, Japan).

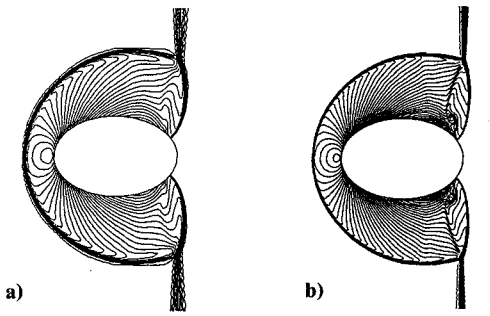


Fig. 5 Mesh-convergence check of computed solutions; a) 361 × 101 mesh, b) 721 × 201 mesh.

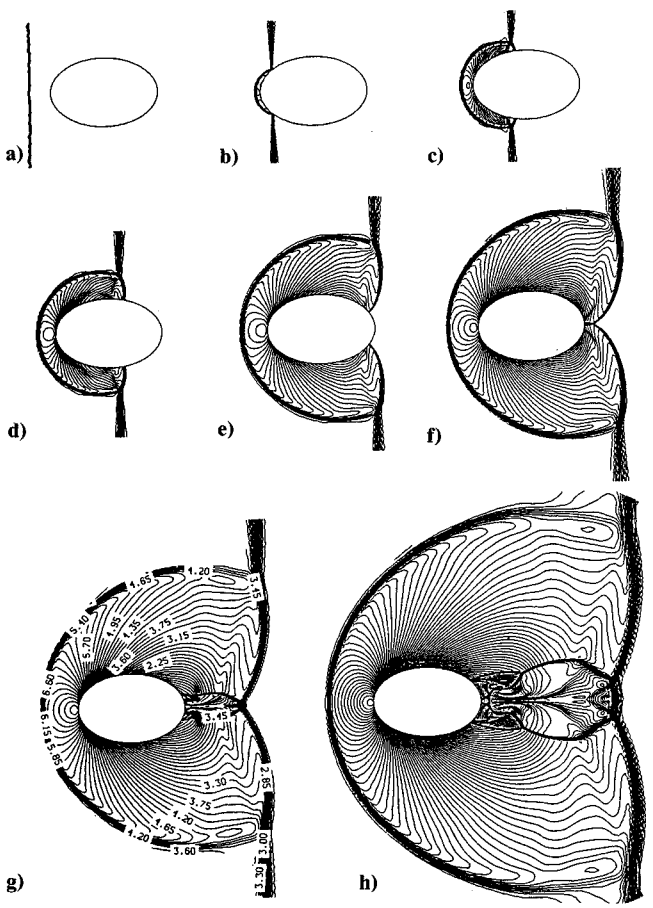


Fig. 6 Computed solution by UNO3 for shock reflection by an elliptic cylinder at $M_s$ = 2.81, sequence of density contours.

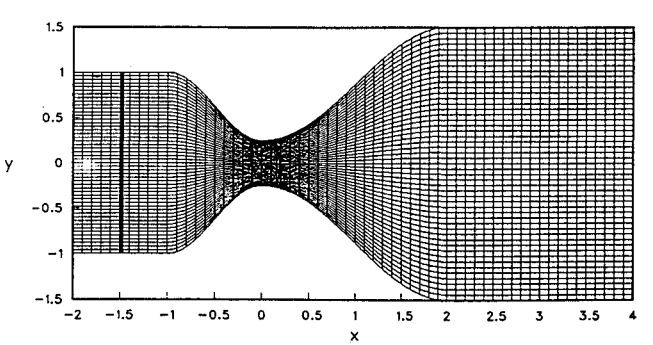


Fig. 7 Geometry and mesh system of a convergent-divergent nozzle.

shock diffraction case, the shock Mach number $M_s$, which represents the strength of the waves, is the dominant factor.

A sequence of computed density contours of the shock diffraction process at a series of times are shown in Fig. 6. In Fig. 6a, the incident shock is about to hit the elliptic cylinder. Fig. 6b–6h shows the subsequent development of the diffraction process that covers regular reflection, transition to Mach reflection, the Mach shocks collision at the wake, and the complex shock-on-shock interactions. The primary incident shock, reflected bow shock, Mach shock, slip lines, and vortex can be easily identified. In general, very good shock-capturing and resolution of the complex flow fields are found in nearly every aspect, except for some viscous effects not accounted for by the Euler equations.

#### Shock Wave Propagating Through a Nozzle

We consider an incident shock wave with shock Mach number $M_s$ = 3.0 propagating through a two-dimensional convergent-divergent nozzle. The nozzle contours are formed by using the sine curves. The geometry of the convergent-divergent nozzle is shown in Fig. 7 and a 301 × 101 grid system is used. The entropy parameter $\varepsilon$ was taken to be 0.1. The ratio of specific heats $\gamma$ is 1.4. This numerical experiment was intended to simulate the unsteady starting process in a shock tunnel. A sequence of density contours at a series of times are shown in Fig. 8. Fig. 8a indicates the regular reflection and Fig. 8b shows the Mach reflection. In Fig. 8c, the reflected bow shocks collide with each other and pass through each other. They proceed further and hit the nozzle walls and are being reflected, see Fig. 8d. The incident Mach shock fronts merge into one propagating shock front and proceeds down the nozzle. The reflected bow waves experience several times reflection by the nozzle walls. The flow fields become extremely complicated due to those multiple interactions of discontinuities (See Figs. 8e–8g). The density contours, pressure contours and Mach number contours corresponding to a later time are shown in Fig. 9. Again, very good capturing of the discontinuities and high resolution of the complex flowfields are observed.

## VI. Concluding Remarks

High resolution nonoscillatory shock-capturing schemes based on reconstruction via the primitive function approach with

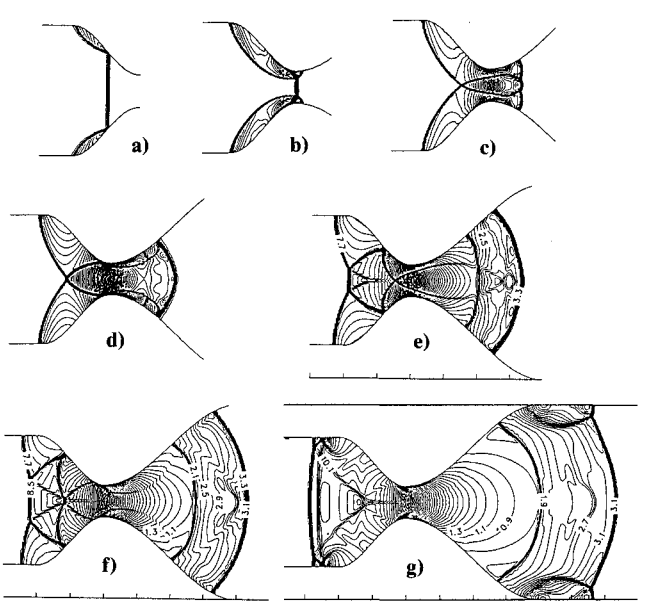


Fig. 8 Computed solution of shock wave propagating through a nozzle $M_s$ = 3.0, sequence of density contours.

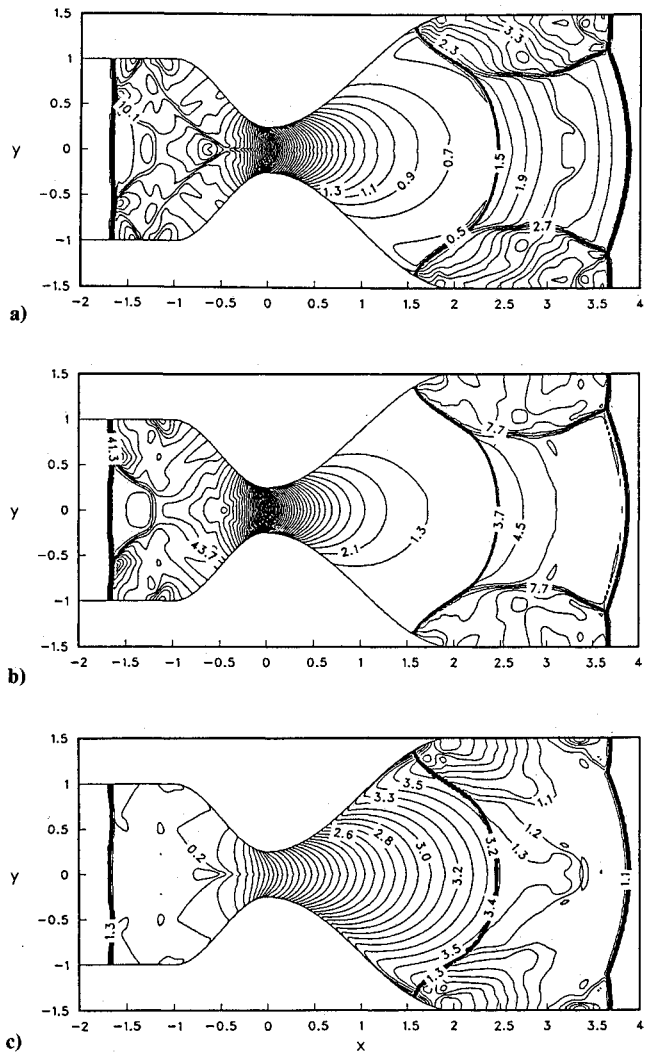


**Fig. 9 Computed solution of shock wave propagating through a nozzle $M_s = 3.0$ at a later time; a) density contours, b) pressure contours, c) mach number contours.**

$N = 3$ have been developed for simulating unsteady compressible Euler equations. Roe's field by field linearization technique was used as the approximate Reimann solver, which permits the use of different flux limiter for each characteristic variable. Numerical results for truly nonstationary shock diffraction by an elliptic cylinder and a shock wave propagating through a convergent-divergent nozzle are obtained. Both problems contain complicated shocks, slip lines, and vortices and their interactions and can be resolved adequately by the proposed scheme. The present third-order (at least in the one-dimensional scalar case) nonoscillatory scheme UNO3 demonstrates its robust stability and high resolution of flowfields.

## Acknowledgments

This work has been supported by the National Science Council, the Republic of China under Grants NSC 78-0210-D002-11 and NSC 79-0410-E002-34. The authors thank T. H. Lee for some of the earlier calculations on the nozzle problem. Many valuable comments and suggestions from the reviewers are gratefully acknowledged.

## References

[1]Yee, H. C., "A Class of High-Resolution Explicit and Implicit Shock-Capturing Methods," NASA TM-101088, Feb. 1989.

[2]Roe, P. L., "Characteristic-based Schemes for the Euler Equations," *Annual Review of Fluid Mechanics*, Vol. 18, 1986, pp. 337–365.

[3]Moretti, G., "Computation of Flows with Shocks," Annual Review of Fluid Mechanics, Vol. 19, 1987, pp. 313–337.

[4]Harten, A., and Osher, S., "Uniformly High-Order Accurate Nonoscillatory Schemes I," *SIAM Journal on Numerical Analysis*, Vol. 24, No. 2, 1987, pp. 279–309.

[5]Harten, A., "Preliminary Results on the Extension of ENO Schemes to Two-Dimensional Problems," *Proceedings of the International Conference on Hyperbolic Problems*, Saint-Etienne, France, Jan. 1986.

[6]Harten, A., Engquist, B., Osher, S., and Chakravarthy, S. R., "Uniformly High Order Accurate Essentially Non-Oscillatory Schemes III," *Journal of Computational Physics*, Vol. 71, No. 2, 1987, pp. 231–303.

[7]Harten, A., Osher, S., Engquist, B., and Chakravarthy, S. R., "Some Results on Uniformly High Order Accurate Essentially Non-Oscillatory Schemes," *Journal of Applied Numerical Mathematics*, Vol. 2, No. 2, 1986, pp. 347–367.

[8]Godunov, S. K., "A Finite Difference Method for the Numerical Computation of Discontinuous Solutions of the Equations of Fluid Dynamics," *Matematicheskii Sbornik*, Vol. 47, 1959, pp. 271–290.

[9]van Leer, B., "Towards the Ultimate Conservative Difference Scheme V, A Second-Order Sequel to Godunov's Method," *Journal of Computational Physics*, Vol. 32, No. 1, 1979, pp. 234–245.

[10]Colella, P., and Woodward, P. R., "The Piecewise-Parabolic Method (PPM) for Gas-Dynamical Simulation," *Journal of Computational Physics*, Vol. 54, No. 1, 1984, p. 174–201.

[11]Harten, A., "High Resolution Schemes for Hyperbolic Conservation Laws," *Journal of Computational Physics*, Vol. 49, No. 2, 1983, pp. 357–393.

[12]Osher, S., and Chakravathy, S. R., "High Resolution Schemes and Entropy Conditions," *SIAM Journal on Numerical Analysis*, Vol. 21, No. 4, 1984, pp. 955–984.

[13]Roe, P. L., "Some Contributions to the Modeling of Discontinuous Flows," *Lecture Notes in Mathematics*, Vol. 22, 1985, pp. 163–193.

[14]Yang, J. Y., "Uniformly Second-Order Essentially Nonoscillatory Schemes for the Euler Equations," *AIAA Journal*, Vol. 28, No. 12, 1990, pp. 2069–2076.

[15]Yang, J. Y., "Third-Order Nonoscillatory Schemes for the Euler Equations," *AIAA Journal*, Vol. 29, No. 10, 1991, pp. 1611–1618.

[16]Roe, P. L., "Approximate Riemann Solvers, Parameter Vectors, and Difference Schemes," *Journal of Computational Physics*, Vol. 43, No. 2, 1981, pp. 357–372.

[17]Strang, G., "On the Construction and Comparison of Difference Schemes," *SIAM Journal of Numerical Analysis*, Vol. 5, No. 3, 1968, pp. 506–517.

[18]Roe, P. L., "A Survey of Upwind Differencing Techniques," *Proceedings of the Eleventh International Conference on Numerical Methods in Fluid Dynamics*, Williamsburg, VA, June 1988.

[19]Yang, J. Y., Liu, Y., and Lomax, H., "Computation of Shock-Wave Reflection by Circular Cylinders," *AIAA Journal*, Vol. 25, No. 5, 1987, pp. 683–689.

[20]Woodward, P., and Colella, P., "The Numerical Simulation of Two-Dimensional Fluid Flow with Strong Shocks," *Journal of Computational Physics*, Vol. 54, No. 1, 1984, pp. 115–173.